PCCP

PAPER

View Article Online
View Journal | View Issue

Cite this: *Phys. Chem. Chem. Phys.*, 2025, **27**, 8764

Carrier-generation mechanism in Zn-doped In_2O_3 transparent conductors†

Sanghyuk Lee,[a] Seungwon Shim,[a] Hyunwoo Jang,[a] Jae Kyeong Jeong [b] and Youngho Kang *[a]

Received 31st January 2025,
Accepted 2nd April 2025

DOI: 10.1039/d5cp00408j

rsc.li/pccp

Zn-doped In_2O_3 (IZO) has been extensively studied as a transparent conducting oxide (TCO) due to its favorable optical and electrical characteristics. In this work, to uncover the origin of degenerate n-type doping in IZO, we investigated point defects using density functional theory (DFT) calculations. Among the two possible configurations of Zn dopants, namely interstitial (Zn_i) and substitutional Zn(Zn_{In}), Zn_{In} is found to be energetically more favorable. While Zn_{In} acts as an acceptor, potentially compensating for n-type doping, it readily forms a defect complex, Zn_{In}–V_O, by combining with oxygen vacancies (V_Os), the dominant intrinsic defects in In_2O_3. This defect complex exhibits a substantial binding energy of approximately 1 eV and functions as a shallow donor. By evaluating carrier concentrations that can occur in IZO films, we demonstrate that the formation of Zn_{In}–V_O is critical to maintaining or even enhancing significant n-type conductivities of IZO. By elucidating the doping behavior of IZO, this work provides critical insights to optimize its properties, thereby helping the advancement of optoelectronic and energy devices where IZO serves as a vital TCO.

1. Introduction

Transparent conducting oxides (TCOs) are indispensable in numerous optoelectronic and energy-harvesting devices, such as liquid crystal displays, light-emitting diodes, and solar cells, owing to their unique combination of metallic conductivity and optical transparency.[1–4] Among TCOs, indium oxide (IO) stands out as a prototype material, offering high carrier concentrations, excellent carrier mobilities, and ease of processing.[5–7] In particular, IO exhibits n-type semiconductor characteristics, with free-electron concentrations reaching up to 10^{20} cm^{-3} even in undoped films.[8–10] Its conductivity can be further improved by incorporating dopants that introduce additional free electrons above the conduction band. Among various doped forms of IO, Sn-doped IO (ITO) is renowned for its exceptionally high conductivity (5.7×10^3 S cm^{-1}), attributed to its extremely high carrier densities exceeding 10^{21} cm^{-3}.[11] Consequently, ITO is the most widely utilized TCO in commercial products.

Zn-doped IO (IZO) is another IO-based TCO that has been extensively studied for its advantages in carrier transport and optical transparency.[12–15] Qiu *et al.* reported that IZO films deposited by radio frequency magnetron sputtering display fairly high carrier mobilities of ~50 cm^2 V^{-1} s^{-1}, which is larger than the value for ITO prepared by the same technique.[12] In addition, IZO films have higher work functions than ITO films, which can improve the performance of solar cells.[12,16] The significant optical transparency is another merit of IZO films; their transmittance for the visible range is higher than 80%, which is comparable to ITO.[14] In particular, IZO has relatively low Urbach tails near the conduction bottom, giving rise to low free-carrier absorption.[12]

Despite its promising properties, a complete understanding of the fundamental aspects of IZO remains elusive. In particular, the carrier-generation mechanism in IZO, which is essential for optimizing its electrical properties, is still not fully understood. Zn has a formal charge of 2+ in oxides, while In has a charge of 3+. When Zn substitutes for In sites in IO, this doping is likely to produce acceptors that counteract inherent n-type doping of IO films. However, IZO with Zn concentrations exceeding 10^{20} cm^{-3} consistently maintain significant free-electron concentrations, even surpassing 10^{20} cm^{-3}.[17,18] More intriguingly, Zn doping sometimes enhances the n-type conductivity.[15,17,19] Additional generation of oxygen vacancies due to the charge difference between Zn^{2+} and In^{3+} has been suggested as a possible origin for the significant n-type conductivity of IZO in literature.[15,20] In a previous work, point defects and n-type doping in IZO were theoretically investigated.[21] However, the study reported low carrier concentrations of ~10^{10} cm^{-3} under equilibrium conditions. To date, the detailed source of free carriers in IZO and the role of Zn dopants have not yet been identified. In addition,

[a] *Department of Materials Science and Engineering, Incheon National University, Incheon 22012, Korea. E-mail: youngho84@inu.ac.kr*
[b] *Department of Electronic Engineering, Hanyang University, Seoul 04763, Korea*
† Electronic supplementary information (ESI) available. See DOI: https://doi.org/10.1039/d5cp00408j

the impact of Zn doping on the atomic and electronic structures remains unexplored.

In this work, we investigate point defects in IZO to elucidate the impact of Zn doping on its electrical properties using density functional theory (DFT) calculations. By comparing the formation energies of Zn interstitials (Zn_i) and substitutional defects replacing In sites (Zn_{In}), we reveal that Zn preferentially forms Zn_{In} over Zn_i. As expected, Zn_{In} acts as an acceptor, which could potentially compensate for n-type doping of IO. However, we find that Zn_{In} readily forms defect complexes Zn_{In}–V_O with oxygen vacancies (V_Os), the dominant intrinsic defects in IO. These Zn_{In}–V_O complexes exhibit a significant binding energy of approximately 1 eV and function as shallow donors. By explicitly calculating the carrier concentration considering experimental growth conditions of IZO films, we demonstrate that these defect complexes play a critical role in maintaining or even enhancing the n-type conductivity of IZO.

2. Computational detail

We performed DFT calculations using Vienna *Ab initio* Simulation Package with projector augmented wave (PAW) pseudopotential.[22,23] For describing the electron–electron interaction, we employed a Heyd–Scuseria–Ernzerhof hybrid functional (HSE06).[24] We use a Hartree–Fock mixing parameter of 0.3 and a screening parameter of 0.2 $Å^{-1}$, which yields a band gap of 2.93 eV for IO, consistent with experimental values.[25] For the Brillouin zone (BZ) integration, a (1/4 1/4 1/4) special k point was used.[26] A cutoff energy for plane-wave basis was set to 500 eV. The criterion to ensure the charge-density convergence was set to 10^{-5} eV. Atomic positions were relaxed until the forces acting on each atom became less than 0.02 eV $Å^{-1}$. Spin-polarization was considered throughout the calculations. We did not consider van der Waals (vdW) effects. The vdW effects are important for simulating molecular systems or low-dimensional materials with weak non-covalent interactions. However, for three-dimensional inorganic solids, their impact is expected to be less significant, and reliable methods for incorporating them have not been established yet.[27] A DFT+U method in which on-site energy U is applied to localized In 4d and Zn 3d states would partly adjust the energy positions of the d states. However, since the d levels in In_2O_3 are fairly deep in energy, the DFT+U method does not effectively correct the band-gap underestimation.[28] Thus, in the present study, we focus on the HSE06 approach, which has been proven accurate in predicting properties of semiconductors and insulators.[29,30]

The formation energy of a defect with a charge (D^q) was obtained by using the following formula:[31]

$$E^f[D^q] = E_{tot}[D^q] - E_{tot}[bulk] - \sum_i n_i\mu_i + qE_F + E_{corr}, \quad (1)$$

where $E_{tot}[D^q]$ and $E_{tot}[bulk]$ are the energies of defective and host supercells, respectively. n_i is the number of i atom to be removed from ($n_i > 0$) and added into ($n_i < 0$) the supercell, and μ_i is the corresponding chemical potential. The chemical potentials μ_{In} and μ_{Zn} are referenced to the per-atom energy of a corresponding bulk metal and μ_0 is referenced to half of the O_2(g) energy. The chemical potential depends on the growth condition. To ensure the phase stability of In_2O_3, we considered $\mu_{In} = 0$ and $\mu_O = 1/3H_f(In_2O_3)$ for O-poor limit while $\mu_{In} = 1/2H_f(In_2O_3)$ and $\mu_O = 0$ for O-rich limit, where $H_f(In_2O_3)$ is the heat of formation of In_2O_3. We accounted for the maximum μ_{Zn} to avoid the precipitation of the ZnO phase [namely, $\mu_{Zn} + \mu_O \leq H_f(ZnO)$, where $H_f(ZnO)$ is the heat of formation of ZnO]. E_F is the Fermi level referenced to the valence band maximum (VBM), which corresponds to the electron chemical potential. E_{corr} is a correction term to fix the finite-size effects of charged supercells. We employed the scheme proposed by Freysoldt *et al.* to obtain E_{corr}.[32] Due to the limited atomic relaxation around a point defect, its formation energy is usually insensitive to the supercell size.[33] Herein, the defect calculations were conducted on a cubic bixbyite lattice ($Ia\bar{3}$) including 16 formula units of In_2O_3. To model a positively(negatively) charged defect, we remove(add) electron(s) from the supercell. The calculated lattice parameter is 10.178 Å which is in good agreement with experiments within 1%.[34–36]

3. Results and discussion

At ambient conditions, In_2O_3 crystallizes into a bixbyite cubic structure, as shown in Fig. 1. Two inequivalent sites for In

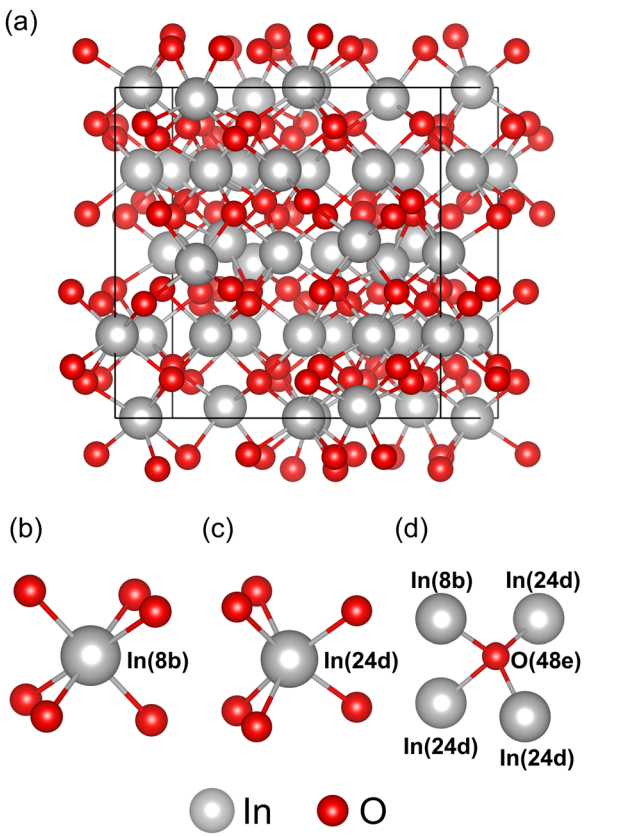

Fig. 1 (a) Crystal structure of bixbyite In_2O_3 and local motifs of In and O. Local motifs for (b) In(8b), (c) In(24d), and (d) O(48e).

(8b and 24d sites in the Wyckoff notation) are present in the bixbyite structure (Fig. 1(b) and (c)), and all of In cations are coordinated with six O anions. On the other hand, all O anions are located on 48e sites (Fig. 1(d)), and they are fourfold coordinated with In cations.

Fig. 2(a)–(c) shows the atomic structures of V_O, Zn_i, and Zn_{In} for their respective charge states, which are stable under n-type conditions with the E_F positioned close to the conduction band minimum (CBM). An oxygen vacancy is an intrinsic donor in IO. Upon an V_O^{2+} is created, the surrounding In cations relax outward by 10% because of the lack of In–O bonds and the resulting repulsive interactions between the cations. We observe that the In neighbors of a V_O defect does not relax inward significantly, even in the neutral and 1+ charge states, which contain electrons in the V_O-induced defect state. Specifically, the relaxation amounts to −0.64% (inward) for V_O^0 and 5.20% (outward) for V_O^+, relative to their equilibrium positions. This relaxation pattern implies the shallow nature of V_O donors in IO. Namely, the electrons occupying the defect state are fairly delocalized in V_O^0 or V_O^+, causing ineffective screening of the repulsion between the cations. This sharply contrasts with the relaxation of neighboring cations around deep V_O defects observed in other oxides. For example, in ZnO, where V_O is known to be a deep donor, the Zn ions surrounding V_O relax inward by 12% in the neutral state.[37] On the other hand, we find that the presence of V_O^{2+} leads to only minor modifications to the band structure, without introducing deep levels within the band gap (Fig. 2(d)). The slight change in the conduction band arises from the mixing between the host and V_O^{2+}-induced states. Nonetheless, the conduction band near the edge still maintains a large dispersion similar to that of pristine IO (green dashed line in Fig. 2(d)), supporting high carrier mobilities of n-type IO films.

When Zn is incorporated into IO, it can form either Zn_i or Zn_{In}. For Zn_i, there are two interstitial sites in the bixbyite structure: 8a and 16c. The Zn_is on these two sites have almost the same formation energies, with the difference being less than 0.1 meV, resulting in similar structural and electrical properties. In the following discussion, we focus on the Zn_i at a 16c site. Zn_i can act as a single or double donor, and Fig. 2(b) depicts the atomic structure of Zn_i^{2+}, where the Zn ion is surrounded by six O ions. Because of the large size of a Zn cation, Zn_i causes significant distortion in the surrounding lattice. In particular, it repels nearby In ions, causing a considerable contraction of In–O bond lengths from 2.19 to 2.14 Å. We notice that Zn_i^{2+} does not develop a defect level inside the band gap, as shown in Fig. 2(e). Instead, the defect state, which relates to the empty Zn 4s level, resides somewhere above the conduction band. Accordingly, the dispersion near the CBM remains largely unchanged compared to that of pristine IO.

On the other hand, Zn can substitute In at either the 8b or 24d site. Similar to Zn_i, the atomic sites for Zn_{In} do not lead to significant changes in the formation energies (with a difference of approximately 0.13 eV) and in the structural and electrical properties of Zn_{In}. We focus on the more stable Zn_{In} at the 24d site below. In contrast to Zn_i, Zn_{In} can serve as a single acceptor. Fig. 2(c) illustrates the atomic configuration of Zn_{In}^-, where the Zn ion is six-fold coordinated with O ions. Due to the smaller ionic radius of Zn compared to In, the substitutional Zn attracts nearby O ions, giving rise to Zn–O bond lengths (∼2.18 Å) shorter than the equilibrium In–O bond lengths

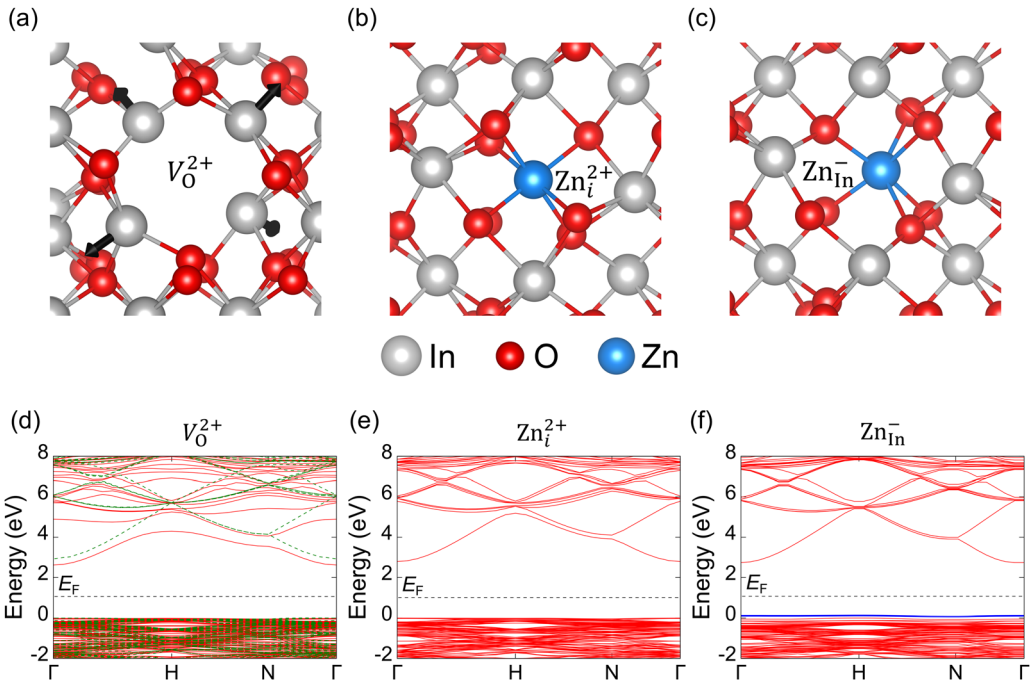

Fig. 2 Atomic structures of (a) V_O^{2+}, (b) Zn_i^{2+}, and (c) Zn_{In}^-. Electronic band structures of (d) V_O^{2+}, (e) Zn_i^{2+}, and (f) Zn_{In}^-. The valence band maximum of undoped In_2O_3 is set to 0. In (a), the arrows indicate the displacement of neighboring In ions. In (d), the green dashed line represents the band structure of pristine In_2O_3. In (f), the blue line represents the defect state induced by Zn_{In}.

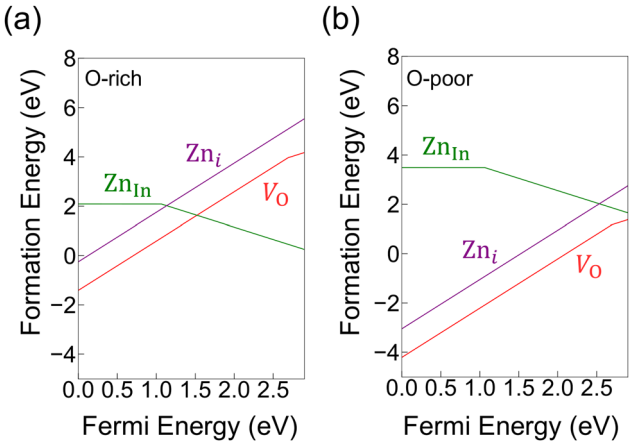

Fig. 3 Defect formation energies as a function of Fermi energy at the (a) O-rich and (b) O-poor limits.

(~2.19 Å) along with a slight change in bond angles. For Zn_{In}^{-}, the defect state that accepts an extra electron lies in the vicinity of the VBM, as shown in Fig. 2(f). This defect state primarily arises from the hybridization between Zn and adjacent O states, exhibiting an antibonding character (partial density of states and charge density analysis are provided in Fig. S1 in the ESI†). As a result, when the transition from Zn_{In}^{0} to Zn_{In}^{-} occurs by accepting an excess electron, compensating for n-type doping, the Zn–O bond lengths somewhat increase from 2.14 to 2.18 Å on average. Similar to Zn_i^{2+}, Zn_{In}^{-} has little impact on the dispersion of the conduction band near the CBM.

We examine the formation energies of the isolated defects discussed above, as shown in Fig. 3. For readability, we present the formation energies for the most stable charge states of each defect at a given Fermi level, which correspond to the slopes of the formation-energy curves. For V_O, it is observed that V_O^{2+} is the most stable over a wide range of the Fermi level. The stability transition from V_O^{2+} to V_O^{+} occurs at 0.24 eV below the CBM, while the stable region for V_O^{0} does not appear within the band gap. This is in good agreement with previous calculations.[38] Consistent with the atomic structures, the higher stability of V_O^{2+} and V_O^{+} relative to V_O^{0} at the Fermi level close to the CBM suggests that V_O is a shallow donor, which can donate free electrons to the conduction band at room temperature once it is created. Notably, V_O displays formation energies less than 1 eV under oxygen-poor limit at $E_F \sim$ CBM. Given that IO films are usually grown under oxygen-deficient environments, oxygen vacancies are therefore expected to be the dominant defects, leading to n-type conductivities.

Zn_i is stabilized in the 2+ charge state at the E_F within the band gap. Therefore, it can act as an effective double donor capable of producing two free electrons when formed. However, its formation energy is fairly high (>2.5 eV) at $E_F \sim$ CBM, regardless of the growth condition, which is attributed to the high energy cost of the significant lattice distortion, as explained in the foregoing discussion. As a result, its concentration should be marginal in n-type IO films. On the other hand, Zn_{In} remains stable in the neutral state up to $E_F \sim 1$ eV, while its negative charge state becomes more energetically favorable at higher E_F. As such, Zn_{In} can play a role as a compensator against n-type doping by accepting an excess electron from the host. The formation energy of Zn_{In} is quite close to that of V_O under oxygen-poor limit at $E_F \sim$ CBM and it can be smaller depending on growth conditions. This result seems to indicate that Zn doping deteriorates the n-type conductivity of IO films due to the formation of Zn_{In} acceptors, which contradicts experimental observations.

On the other hand, in extremely doped semiconductors with dopant concentrations exceeding 10^{19} cm^{-3}, point defects may form defect complexes to decrease the enthalpy of the system despite the reduction of configurational entropy.[39,40] In IZO, Zn_{In} can form a defect complex, Zn_{In}–V_O, by combining with V_O, a dominant intrinsic defect, as shown in Fig. 4(a). To assess the feasibility of defect-complex formation, we examine the binding energy (E_b) using the following equation:

$$E_b = E^f(Zn_{In}) + E^f(V_O) - E^f(Zn_{In}\text{–}V_O). \quad (2)$$

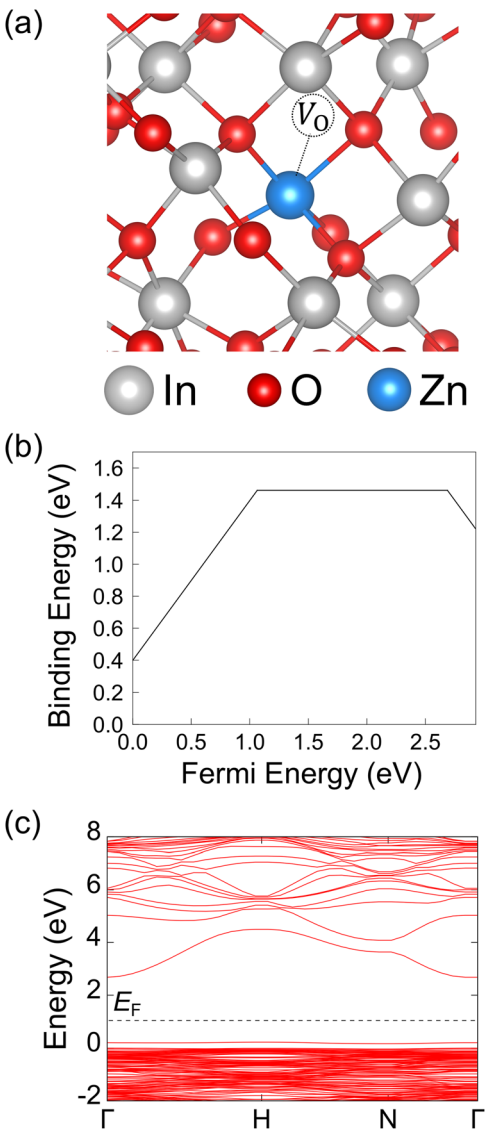

Fig. 4 (a) Atomic structure, (b) binding energy, and (c) band structure for $(Zn_{In}–V_O)^+$. In (c), the valence band maximum of pristine In_2O_3 is set to 0.

The most stable charge state for each defect at a given Fermi level is considered when calculating the binding energy in eqn (2). As a result, E_b depends on the E_F position. Notably, Fig. 4(b) shows that Zn_{In}–V_O has large positive binding energies over 1 eV under n-type conditions, indicating that formation of the defect complex is highly favorable. The significant binding energy originates from the electrostatic attraction between V_O^+ and Zn_{In}^-. (We examined other sites for V_O in the supercell and confirmed that the configuration discussed above is the most stable.) Furthermore, the band structure of Zn_{In}–V_O (Fig. 4(c)) shows that the defect complex is a shallow donor, which does not produce a deep level to trap electrons. As such, it is likely to be a possible n-type source that can explain the puzzling doping behavior of Zn doped In_2O_3.

To firmly confirm the role of Zn_{In}–V_O, we explicitly evaluate the carrier (n_e) and defect [D^q] concentrations considering experimental synthesis conditions of IO films. We calculate n_e as

$$n_e = N_C \exp\left(-\frac{CBM - E_F}{kT}\right), \quad (3)$$

where N_C is the effective density of states, which is set to 5.9×10^{18} cm^{-3} considering the calculated electron effective mass ($0.23m_0$, where m_0 is the electron rest mass). g is the structural degeneracy factor of a given defect, which is set to 1 for isolated defects and 6 for the defect complex. k is the Boltzmann constant and T is the temperature, which is set to 500 K, reflecting an experimental annealing temperature applied to IO films.[41] [D^q] is obtained by

$$[D^q] = N_D g \exp\left(-\frac{E_F(D^q)}{kT}\right), \quad (4)$$

where N_D denotes the concentration of atomic sites available for defect formation. To determine n_e and [D^q], it is essential to identify the Fermi level at which the charge neutrality condition (CNC) among charged species is satisfied. In this work, the CNC can be expressed as:

$$[V_O^+] + 2[V_O^{2+}] + [(Zn_{In}\text{–}V_O)^+] \rightarrow [Zn_{In}^-] + n_e. \quad (5)$$

In eqn (5), we neglect the concentrations of hole and other defects such as Zn_i^+, which are expected to be negligible. Typically, transparent conductors based on undoped IO films exhibit carrier concentrations in the range of 10^{19}–10^{20} cm^{-3} in experiments.[8–10] To reflect this observation, we consider chemical potentials of In and O that yield a calculated carrier concentration of approximately 2.0×10^{19} cm^{-3} for undoped IO. These chemical potentials fall outside the oxygen-poor limit previously discussed in Fig. 3, suggesting that the synthesized IO films exist in a nonequilibrium state, potentially leading to the occurrence of secondary phases. It is worth noting that degenerate semiconductor thin films, such as TCOs and P-doped Si used as source and drain materials in transistors,[42,43] are usually produced using nonequilibrium growth techniques. Nevertheless, such films remain kinetically stable, enabling reliable device operation.

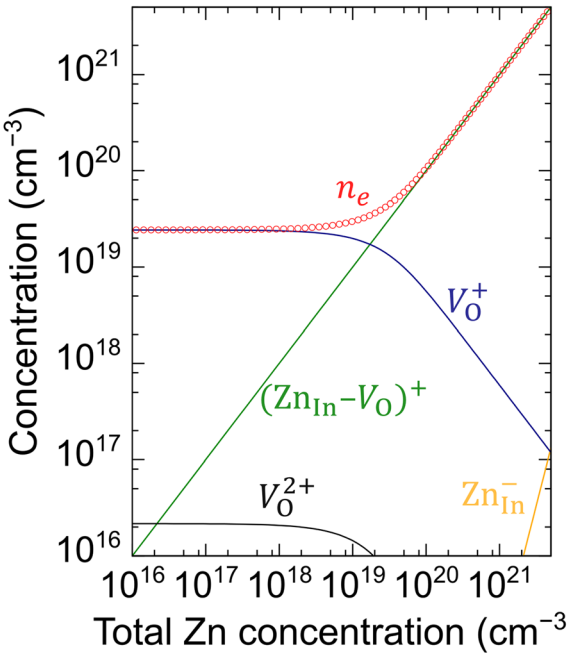

Fig. 5 Calculated concentrations of V_O^+, V_O^{2+}, Zn_{In}^-, $(Zn_{In}–V_O)^+$, and free electrons as a function of Zn doping level.

Fig. 5 shows the calculated n_e and [D^q] as a function of the total Zn concentration (*i.e.*, $[Zn_{In}^-] + [(Zn_{In}–V_O)^+]$). It should be noted that, between Zn_{In}^- and $(Zn_{In}–V_O)^+$, the latter is the dominant form; most of the Zn doped into IO forms the defect complex, while the concentration of isolated Zn_{In}^- is insignificant. This is attributed to the considerable binding energy of $(Zn_{In}–V_O)^+$, as mentioned above. At low Zn doping levels (10^{16}–10^{18} cm^{-3}), the predominant point defect is V_O^+, and the free-electron concentration n_e closely matches $[V_O^+]$. However, as the Zn doping level increases beyond $\sim 10^{19}$ cm^{-3}, the concentrations of isolated oxygen vacancies ($[V_O^+]$ and $[V_O^{2+}]$) begin to decline, while the concentration of $(Zn_{In}–V_O)^+$ continues to increase, becoming the dominant defect. As a result, $(Zn_{In}–V_O)^+$ serves as a major donor that produces free carriers, enabling higher carrier concentrations than that of undoped IO. Our findings clearly demonstrate that Zn doping is not detrimental to n-type doping of IO films due to the favorable formation of the defect complex, which allows for the maintenance or even enhancement of carrier concentrations.

4. Conclusions

We performed first-principles calculations to investigate the impact of Zn doping on n-type doping in indium oxide. Among the two possible isolated Zn defects, Zn_i and Zn_{In}, Zn_{In} is energetically more favorable. Our analysis of the electronic structure and formation energy revealed that Zn_{In} acts as an acceptor. However, it readily forms the defect complex Zn_{In}–V_O by combining with oxygen vacancies, the predominant native defects in IO. This defect complex exhibits a significant binding energy and functions as a shallow donor, playing a critical role

in sustaining n-type doping of IO. Our calculation of carrier concentrations further confirmed that the formation of Zn_{In}–V_O is a key to the carrier-generation mechanism in Zn-doped IO films. By shedding light on the doping behavior of IZO, this work provides important insights into optimizing the electrical properties of IZO films, thereby aiding the advancement of optoelectronic and energy devices in which IZO serves as a vital transparent conducting oxide.

Data availability

The data supporting this article has been included as part of the ESI.†

Conflicts of interest

There are no conflicts of interest to declare.

Acknowledgements

This research was supported by the National Research Foundation (NRF) funded by the Korean government (MSIT) (No. RS-2024-00407840).

References

1 H. Liu, V. Avrutin, N. Izyumskaya, Ü. Özgür and H. Morkoç, Transparent Conducting Oxides for Electrode Applications in Light Emitting and Absorbing Devices, *Superlattices Microstruct.*, 2010, **48**(5), 458–484.
2 H. Hosono, Recent Progress in Transparent Oxide Semiconductors: Materials and Device Application, *Thin Solid Films*, 2007, **515**(15), 6000–6014.
3 Z. Chen, J. Wang, H. Wu, J. Yang, Y. Wang, J. Zhang, Q. Bao, M. Wang, Z. Ma, W. Tress and Z. Tang, A Transparent Electrode Based on Solution-Processed ZnO for Organic Optoelectronic Devices, *Nat. Commun.*, 2022, **13**(1), 4387.
4 H. Kim, C. M. Gilmore, A. Piqué, J. S. Horwitz, H. Mattoussi, H. Murata, Z. H. Kafafi and D. B. Chrisey, Electrical, Optical, and Structural Properties of Indium–Tin–Oxide Thin Films for Organic Light-Emitting Devices, *J. Appl. Phys.*, 1999, **86**(11), 6451–6461.
5 F. Alam and D. J. Lewis, Synthesis of Indium Oxide Microparticles Using Aerosol Assisted Chemical Vapour Deposition, *RSC Adv.*, 2020, **10**(38), 22487–22490.
6 M. A. Flores-Mendoza, R. Castanedo-Perez, G. Torres-Delgado, J. Márquez Marín and O. Zelaya-Angel, Influence of the Annealing Temperature on the Properties of Undoped Indium Oxide Thin Films Obtained by the Sol–Gel Method, *Thin Solid Films*, 2008, **517**(2), 681–685.
7 H. Jang, S. Shim, J. Son and Y. Kang, Bi(III)-based oxide semiconductors with ambipolar doping: (Na, K)BiO_2, *J. Am. Ceram. Soc.*, 2024, **107**(9), 6285–6293.
8 A. Dixit, C. Sudakar, R. Naik, V. M. Naik and G. Lawes, Undoped Vacuum Annealed In_2O_3 Thin Films as a Transparent Conducting Oxide, *Appl. Phys. Lett.*, 2009, **95**(19), 192105.
9 Z.-X. Zhang, M.-J. Zhao, W.-Y. Wu, D.-S. Wuu, P. Gao, S. Y. Lien and W. Z. Zhu, Two-Regime Property Dependence on Plasma Power of Plasma-Enhanced Atomic Layer-Deposited In_2O_3 Thin Films and Underlying Mechanism, *Vacuum*, 2023, **216**, 112414.
10 Y. Magari, T. Kataoka, W. Yeh and M. Furuta, High-Mobility Hydrogenated Polycrystalline In_2O_3 (In_2O_3:H) Thin-Film Transistors, *Nat. Commun.*, 2022, **13**(1), 1078.
11 Y. Ren, P. Liu, R. Liu, Y. Wang, Y. Wei, L. Jin and G. Zhao, The Key of ITO Films with High Transparency and Conductivity: Grain Size and Surface Chemical Composition, *J. Alloys Compd.*, 2022, **893**, 162304.
12 Q. Qiu, Y. Bai, J. Li, C. Guo, H. Chen, H. Zhang, J. Shi, W. Liu, T. Chen, J. Liao and J. Yu, ZnO-Doped In_2O_3 Front Transparent Contact Enables >24.0% Silicon Heterojunction Solar Cells, *Energy Technol.*, 2023, **11**(4), 2201310.
13 S. Li, Z. Shi, Z. Tang and X. Li, Comparison of ITO, In_2O_3:Zn and In_2O_3:H Transparent Conductive Oxides as Front Electrodes for Silicon Heterojunction Solar Cell Applications, *Vacuum*, 2017, **145**, 262–267.
14 M. Morales-Masis, S. M. De Nicolas, J. Holovsky, S. De Wolf and C. Ballif, Low-Temperature High-Mobility Amorphous IZO for Silicon Heterojunction Solar Cells, *IEEE J. Photovolt.*, 2015, **5**(5), 1340–1347.
15 A. Jannat, N. Syed, K. Xu, M. A. Rahman, M. M. M. Talukder, K. A. Messalea, M. Mohiuddin, R. S. Datta, M. W. Khan, T. Alkathiri, B. J. Murdoch, S. Z. Reza, J. Li, T. Daeneke, A. Zavabeti and J. Z. Ou, Printable Single-Unit-Cell-Thick Transparent Zinc-Doped Indium Oxides with Efficient Electron Transport Properties, *ACS Nano*, 2021, **15**(3), 4045–4053.
16 A. Chen and K. Zhu, Effects of TCO Work Function on the Performance of TCO/n-Si Hetero-Junction Solar Cells, *Sol. Energy*, 2014, **107**, 195–201.
17 M. Jothibas, C. Manoharan, S. Ramalingam, S. Dhanapandian and M. Bououdina, Spectroscopic Analysis, Structural, Microstructural, Optical and Electrical Properties of Zn-Doped In_2O_3 Thin Films, *Spectrochim. Acta, Part A*, 2014, **122**, 171–178.
18 N. Beji, M. Souli, S. Azzaza, S. Alleg and N. Kamoun Turki, Study on the Zinc Doping and Annealing Effects of Sprayed In_2O_3 Thin Films, *J. Mater. Sci.: Mater. Electron.*, 2016, **27**, 4849–4860.
19 H. Hara, T. Shiro and T. Yatabe, Optimization and Properties of Zn Doped Indium Oxide Films on Plastic Substrate, *Jpn. J. Appl. Phys.*, 2004, **43**, 745.
20 N. Singh, C. Yan and P. S. Lee, Room Temperature CO Gas Sensing Using Zn-Doped In_2O_3 Single Nanowire Field Effect Transistors, *Sens. Actuators, B*, 2010, **150**(1), 19–24.
21 Z. G. Yu, J. Sun, M. B. Sullivan, Y.-W. Zhang, H. Gong and D. J. Singh, Dopant chemical potential modulation on oxygen vacancies formation in In_2O_3: A comparative density functional study, *Chem. Phys. Lett.*, 2015, **621**, 141–145.
22 G. Kresse and J. Furthmüller, Efficient Iterative Schemes for Ab Initio Total-Energy Calculations Using a Plane-Wave Basis Set, *Phys. Rev. B: Condens. Matter Mater. Phys.*, 1996, **54**(16), 11169–11186.

23 G. Kresse and D. Joubert, From Ultrasoft Pseudopotentials to the Projector Augmented-Wave Method, *Phys. Rev. B: Condens. Matter Mater. Phys.*, 1999, **59**(3), 1758–1775.
24 J. Heyd, G. E. Scuseria and M. Ernzerhof, Hybrid Functionals Based on a Screened Coulomb Potential, *J. Chem. Phys.*, 2003, **118**(18), 8207–8215.
25 P. D. C. King, T. D. Veal, F. Fuchs, C. Y. Wang, D. J. Payne, A. Bourlange, H. Zhang, G. R. Bell, V. Cimalla, O. Ambacher, R. G. Egdell, F. Bechstedt and C. F. McConville, Band gap, electronic structure, and surface electron accumulation of cubic and rhombohedral In_2O_3, *Phys. Rev. B: Condens. Matter Mater. Phys.*, 2009, **79**(20), 205211.
26 Y. Kang, B. D. Ahn, J. H. Song, Y. G. Mo, H.-H. Nahm, S. Han and J. K. Jeong, Hydrogen Bistability as the Origin of Photo-Bias-Thermal Instabilities in Amorphous Oxide Semiconductors, *Adv. Electron. Mater.*, 2015, **1**(7), 1400006.
27 E. F. Lima and T. Bredow, Extended benchmark set for lattice parameters of inorganic solids, *J. Comput. Chem.*, 2024, **45**(32), 2702–2709.
28 A. Posada-Borbón and H. Grönbeck, Hydrogen adsorption on In_2O_3(111) and In_2O_3(110), *Phys. Chem. Chem. Phys.*, 2020, **22**(28), 16193–16202.
29 M. Mohamed, C. Janowitz, I. Unger, R. Manzke, Z. Galazka, R. Uecker, R. Fornari, J. R. Weber, J. B. Varley and C. G. Van de Walle, The electronic structure of β-Ga_2O_3, *Appl. Phys. Lett.*, 2010, **97**(21), 211903.
30 A. Alkauskas, B. B. Buckley, D. D. Awschalom and C. G. Van de Walle, First-principles theory of the luminescence lineshape for the triplet transition in diamond NV centres, *New J. Phys.*, 2014, **16**(7), 073026.
31 C. Freysoldt, B. Grabowski, T. Hickel, J. Neugebauer, G. Kresse, A. Janotti and C. G. Van de Walle, First-Principles Calculations for Point Defects in Solids, *Rev. Mod. Phys.*, 2014, **86**(1), 253–305.
32 C. Freysoldt, J. Neugebauer and C. G. Van de Walle, Fully Ab Initio Finite-Size Corrections for Charged-Defect Supercell Calculations, *Phys. Rev. Lett.*, 2009, **102**(1), 016402.
33 R. Vidya, P. Ravindran, H. Fjellvåg, B. G. Svensson, E. Monakhov, M. Ganchenkova and R. M. Nieminen, Energetics of intrinsic defects and their complexes in ZnO investigated by density functional calculations, *Phys. Rev. B: Condens. Matter Mater. Phys.*, 2011, **83**(4), 045206.
34 D. R. Hagleitner, M. Menhart, P. Jacobson, S. Blomberg, K. Schulte, E. Lundgren, M. Kubicek, J. Fleig, F. Kubel, C. Puls, A. Limbeck, H. Hutter, L. A. Boatner, M. Schmid and U. Diebold, Bulk and Surface Characterization of In_2O_3 (001) Single Crystals, *Phys. Rev. B: Condens. Matter Mater. Phys.*, 2012, **85**(11), 115441.
35 C. Y. Wang, Y. Dai, J. Pezoldt, B. Lu, T. Kups, V. Cimalla and O. Ambacher, Phase Stabilization and Phonon Properties of Single Crystalline Rhombohedral Indium Oxide, *Cryst. Growth Des.*, 2008, **8**(4), 1257–1260.
36 A. Bouhdjer, H. Saidi, A. Attaf, A. Yahia, M. S. Aida, O. Benkhetta and L. Bouhdjer, Effects of Lattice Mismatches in In_2O_3/Substrate Structures on the Structural, Morphological and Electrical Properties of In_2O_3 Films, *Surf. Interfaces*, 2020, **20**, 100579.
37 A. Janotti and C. G. Van de Walle, Oxygen vacancies in ZnO, *Appl. Phys. Lett.*, 2005, **87**(12), 122102.
38 I. Chatratin, F. P. Sabino, P. Reunchan, S. Limpijumnong, J. B. Varley, C. G. Van de Walle and A. Janotti, Role of point defects in the electrical and optical properties of In_2O_3, *Phys. Rev. Mater*, 2019, **3**(7), 074604.
39 C. G. Van de Walle and J. Neugebauer, First-Principles Calculations for Defects and Impurities: Applications to III-Nitrides, *J. Appl. Phys.*, 2004, **95**(8), 3851–3879.
40 Y. Kang and C. G. Van de Walle, Electrical Compensation Mechanism in Fluorine-Doped SnO_2, *Appl. Phys. Lett.*, 2017, **111**(15), 152107.
41 Z. Yuan, X. Zhu, X. Wang, X. Cai, B. Zhang, D. Qiu and H. Wu, Annealing Effects of In_2O_3 Thin Films on Electrical Properties and Application in Thin Film Transistors, *Thin Solid Films*, 2011, **519**(10), 3254–3258.
42 H.-J. Gossmann, C. S. Rafferty and P. Keys, Junctions for Deep Sub-100 NM MOS: How Far Will Ion Implantation Take Us?, *MRS Online Proc. Libr.*, 2000, **610**, B1–2.
43 S. Shim, H. Jang and Y. Kang, Why Te Doping Can Break the Traditional N-Type Doping Limit of Silicon, *Inorg. Chem.*, 2023, **62**(48), 19734–19740.